

The universal visitation law of human mobility

Markus Schläpfer^{1,2,3,†}, Lei Dong^{1,4,†,*}, Kevin O’Keeffe^{1,†}, Paolo Santi^{1,5}, Michael Szell^{1,6,7}, Hadrien Salat^{3,8}, Samuel Anklesaria¹, Mohammad Vazifeh¹, Carlo Ratti^{1,‡}, Geoffrey B. West^{2,‡}

¹*Senseable City Laboratory, Massachusetts Institute of Technology, Cambridge, Massachusetts 02139, USA*

²*Santa Fe Institute, Santa Fe, New Mexico 87501, USA*

³*Future Cities Laboratory, Singapore-ETH Centre, ETH Zurich, Singapore 138602, Singapore*

⁴*Institute of Remote Sensing and Geographical Information Systems, School of Earth and Space Sciences, Peking University, Beijing 100871, China*

⁵*Istituto di Informatica e Telematica del CNR, Pisa 56124, Italy*

⁶*IT University of Copenhagen, Copenhagen 2300, Denmark*

⁷*ISI Foundation, Turin 10126, Italy*

⁸*Sociology and Economics of Networks and Services, Orange Labs, Châtilion 92320, France*

[†]*Contributed equally to the research.*

[‡]*Contributed equally as senior authors.*

*Email: arch.dongl@gmail.com (L.D.).

Human mobility impacts many aspects of a city, from its spatial structure^{1–3} to its response to an epidemic^{4–7}. It is also ultimately key to social interactions⁸, innovation^{9,10}, and productivity¹¹.

However, our quantitative understanding of the aggregate movements of individuals has remained incomplete. Existing models, such as the gravity law^{12,13} or the radiation model¹⁴, concentrate on the purely spatial dependence of mobility flows but do not capture the varying frequencies of recurrent visits to the same location. Here, we reveal a simple and robust scaling law captures the temporal and spatial spectrum of population movement on the basis of large-scale mobility data from diverse cities around the globe. According to such law, the number of visitors to any location decreases as the inverse square of the product of their visiting frequency and travel distance. We further show that the spatio-temporal flows to different locations give rise to prominent spatial clusters whose area distribution follows Zipf’s law¹⁵. Finally, we build an individual mobility model based on exploration and preferential return to provide a mechanistic explanation for the discovered scaling law and the emerging spatial structure. Our findings corroborate long-standing conjectures in human geography (such as central place theory¹⁶ and Weber’s theory of emergent optimality¹⁰) and allow for predictions of recurrent flows, providing a basis for application in urban planning, traffic engineering, and the mitigation of epidemic diseases.

The movement of people is fundamental to our societies: it enables social, economic and cultural exchanges^{8,17–19}, shapes the form of cities^{1,20,21}, gives rise to traffic congestion and pollution²², and fuels the spread of contagious diseases^{7,23}. For all these aspects, it is crucial to understand not only how many individuals move from place to place, but also how often they do so. Indeed, since places

attract individuals for reasons as diverse as work, shopping or recreation, mobility fluxes span a wide range of both temporal and spatial scales, from daily visits within the same neighbourhood to once-in-a-lifetime visits that require travel across continents^{24,25}. It is this heterogeneity of trips that dictates the rate at which individuals from different neighbourhoods, regions or parts of the world share the same space and may interact with each other.

However, despite this importance, our understanding of the flows of individuals to locations has remained surprisingly incomplete. Existing large-scale mobility studies²⁵ and state-of-the-art models such as the gravity law^{12,13}, the radiation model¹⁴, and related approaches^{26–29} concentrate on the spatial dependence of population flows (e.g., the aggregate number of individuals travelling between two locations) and do not consider recurrent movements associated with varying frequency of visitation; i.e., the question of how the number of visitors to a location depends on their visitation frequency has remained largely unanswered. At the same time, fine-grained models for the mobility behaviour of individuals^{30,31}, such as the exploration and preferential return model³² or the recently proposed container model³³, reproduce the frequency with which a single individual visits different locations. However, the link between this microscopic behaviour and the temporal spectrum of recurrent mobility fluxes arising from an entire population is missing. This ignorance of the temporal spectrum of flows may lead to misconceptions of the spatial mixing of individuals, and thus may have far-reaching practical consequences for the mitigation of epidemic spreading, for urban planning, infrastructure design, and many other applications.

Here we address this gap and decompose the flows of individuals into the underlying dis-

tribution of both travel distance and visitation frequency, allowing us to simultaneously consider the spatial and temporal spectrum of mobility fluxes. We find a powerful scaling law that governs the number of visitors to any location based on how far they are travelling and how often they are visiting. A microscopic model shows that the discovered scaling law accords well with the exploration and preferential return mechanism of individual mobility, establishing a link between periodic movements at the individual level and the resulting flows at the population level. The visitation law opens up unprecedented possibilities to accurately predict flows between locations, and it provides large-scale empirical support for well-established yet largely untested conjectures in human geography (i.e., central place theory and Weber's theory of emergent optimality). Our findings are derived based on the analysis of mobility data from millions of anonymised mobile phone users in highly diverse urban regions across the world (see 'Data description' in Methods): Greater Boston in the United States (North America), Lisbon, Porto and Braga in Portugal (Europe), Singapore (Asia), Dakar in Senegal (Africa) and Abidjan in Ivory Coast (Africa).

Distance-frequency scaling of spectral population flows

To explore both spatial and temporal components of recurrent population flows, we partitioned each geographical region into a high-resolution square grid (depending on the granularity of the data set, we used $500\text{m} \times 500\text{m}$ cells for Greater Boston and Singapore and $1\text{km} \times 1\text{km}$ cells for all other regions; see Methods) and estimated the home location of each mobile phone user, being defined as the grid cell in which the user spent most of the time at night (Methods). We then determined for each location i the set of unique users who visited the corresponding cell and

grouped them according to the distance r of their home location (using distance bins of equal length $\delta r = 1\text{km}$, Fig. 1a) and according to their visitation frequency f (number of days over a period T during which they visited for a minimum duration τ , see Methods). Finally, to factor out effects of area size, we normalised the resulting visitor counts, $N_i(r, f)$, by the area of their origin, giving $\rho_i(r, f) = N_i(r, f)/\mathcal{A}(r)$, with $\mathcal{A}(r) \approx 2\pi r\delta r$. We will refer to the quantity $\rho_i(r, f)$ as the ‘spectral’ flow since we essentially decompose an aggregate population flow from a given distance into its underlying frequency spectrum. We now show that $\rho_i(r, f)$ does not depend on r and f separately, but on the single rescaled variable rf .

We start by illustrating the behaviour of $\rho_i(r, f)$ with the example of Back Bay West, a central location in Boston (Fig. 1a). The distribution of the spectral flows spans a wide range of distance and frequency values. For a fixed frequency f , the values of $\rho_i(r, f)$ systematically decrease with travel distance r (Fig. 1b), which is a well-known feature of aggregate flows^{12,13,25} that do not explicitly distinguish between different frequencies of travel. Similarly, for a fixed distance r , the flows $\rho_i(r, f)$ decrease systematically with increasing visitation frequency f (Fig. 1c) – frequent visitors to a location tend to be outnumbered by infrequent visitors. Strikingly, a close comparison of Fig. 1b and Fig. 1c reveals that, apart from noise in the data, $\rho_i(r, f)$ scales identically with r and f ; that is, $\rho_i(\lambda r, f) \approx \rho_i(r, \lambda f)$ for any r, f and dimensionless factor $\lambda > 0$. As a consequence of this symmetry, the data collapse onto a single curve when plotted against the rescaled variable rf (Fig. 1d), which shows that the spectral flows are actually a function of the single variable rf . Extending this analysis to tens of thousands of locations in our data sets demonstrates that the same distance-frequency scaling is valid in very different urban systems across the world (Fig. 1e,

Extended Data Figs. 1-6 and Supplementary Figs. S4-S18) and is well reproduced by a power law of the form

$$\rho_i(r, f) = \frac{\mu_i}{(rf)^\eta}, \quad (1)$$

with scaling exponent $\eta \approx 2$. The proportionality constant μ_i determines the magnitude of the flows and thus reflects the location-specific ‘attractiveness’. The discovered scaling relation is truly remarkable since the regularity is mostly unaffected by location-specific conditions, including strong variations in surrounding population densities or in the level of economic or infrastructural development.

The universality of equation (1) calls for a simple theoretical argument for the attraction of individuals to locations: the willingness to visit a particular destination is primarily due to the commonly shared interest for its characteristics, and is thus approximately constant across all origins. Indeed, for a fixed destination, the inverse square law revealed here (equation (1) with $\eta = 2$) is equivalent to $1/2\rho v^2 \equiv \text{const.}$, where the combined variable $v := rf$ corresponds to the individuals’ average velocity towards the destination (the effective distance they cover per unit of time to get there). This relation can then be interpreted as the physical manifestation of the constant collective effort (quantified by the energy term $1/2\rho v^2$) that people are willing to make to visit the location (this argument is derived in detail from the standard equation of motion in Supplementary Information section III).

As a direct consequence of the discovered visitation law, we expect that the effective distance covered per visitor over time, $\langle d \rangle_i$, to get to a given destination i , does not depend on the

attractiveness μ_i of the location. More precisely, $\langle d \rangle_i = d_i^{\text{tot}} / N_i^{\text{tot}}$, where d_i^{tot} is the effective distance travelled towards location i , summed over all its visitors, N_i^{tot} , and accumulated over an observation period T (Methods). Figure 2 confirms that the values of $\langle d \rangle_i$ are indeed statistically invariant across space, so that the effective distance travelled per visitor and time unit constitutes a conserved quantity. This invariance might be surprising because it means that more attractive places differ only in the larger number of visitors they receive. They do not increase, however, the effective distance travelled per visitor, as one might expect.

Spatial distribution of the attractiveness

The spatial distribution of the location-dependent attractiveness μ_i , obtained from the data through linear regression of the log-transformed values of equation (1), is depicted in Fig. 3a for Greater Boston. We observe prominent spatial clusters, where larger clusters with higher values of μ_i (e.g., the city of Boston) tend to be surrounded by smaller clusters with lower values of μ_i . This formation of centres and sub-centres is consistent with the literature on urban structure^{20,21,34} as well as with previous empirical studies of urban mobility^{35,36}, being largely explained by the agglomeration effect of cities (i.e. the tendency of businesses and facilities to cluster). To characterise the size distribution of these clusters in terms of their area, we applied the City Clustering Algorithm (CCA)^{37,38}. First, all attractiveness values less than a minimum value μ^* are set to zero. Second, locations with non-zero values that are contiguous in space are merged recursively until all locations with non-zero values belong to one specific cluster. We determined the threshold μ^* by plotting the ratio of the area of the largest cluster to the sum of the areas of all clusters formed

for different μ^* (Fig. 3b), providing a critical value of μ^* where the ratio is minimised. This value marks the onset of the emergence of a single giant cluster and thus serves as a natural choice of μ^* . We then ranked the clusters by their area, so that $Rank = 3$ represents the third-largest cluster, and find that the area distribution is well approximated by $Size \sim Rank^\zeta$ with rank-size exponent $\zeta = -1.17$ (Fig. 3d). This shows that the area distribution of the clusters follows Zipf's law (exponent of ≈ -1), a fundamental regularity in city science that generally applies to the population and area distribution of cities^{39,40}.

Microscopic model of spectral population flows

Our empirical analysis reveals that (1) spatio-temporal population flows to locations follow a highly reproducible scaling law and (2) while the magnitudes of these flows vary substantially across locations, they exhibit a systematic spatial clustering. We now present a model that predicts these two key observations from the mobility behaviour of individuals. To capture the main mechanisms of individual mobility, we use the well-known exploration and preferential return (EPR) model³² as a starting point. At each time step, an individual (agent) chooses, with a certain probability, to either explore a new, previously unvisited location or, with complementary probability, to return to one of the previously visited locations (with a preference for those locations that the agent visited more often). If the agent decides to explore a new location, the radial distance Δr of such displacement is drawn from a heavy-tailed jump-size distribution $P(\Delta r) \sim |\Delta r|^{-1-\alpha}$ with displacement exponent $\alpha \approx 0.55$, while the direction (angle) θ is drawn from a uniform distribution $\theta \sim (2\pi)^{-1}$ (see Methods). Numerical simulation of a population of agents on a regular

square grid demonstrates that the EPR model indeed generates the distance-frequency scaling of the flows to individual locations (key observation 1) with a scaling exponent of $\eta \approx 2$, which is in excellent agreement with the empirical observations (Extended Data Fig. 7). However, since the agents choose their locations independently of each other, the EPR model is unable to reproduce the heterogeneity in the attractiveness of locations and their systematic spatial clustering (key observation 2). In reality, the trajectories of individuals are not independent but spatially coupled through common attraction points⁴¹: people tend to go to popular places (e.g., a shopping area) that are frequented by others. Thus, by ignoring this coupling of the agents' motion, the EPR model generates attractiveness values μ_i that are rather homogeneous and uniform across space (Extended Data Fig. 7), in systematic conflict with the empirical observations (Fig. 3a).

To resolve this discrepancy, we couple the agents' motion in the model so that, when exploring new locations, they are preferentially attracted towards highly frequented areas. To that end, the radial jump distance Δr is still sampled from the same distribution as in the original EPR model, but the direction θ is no longer drawn uniformly at random. Instead, directions towards regions of high visitation are preferentially selected as follows. Let, for a given cell i , $\tilde{d}_i(\theta; R)$ be the effective distance travelled by all agents to all cells within distance R and between angles θ and $\theta + d\theta$ (the quantity \tilde{d}_i thus measures the visitation level of the cells in each direction in terms of the travel efforts by the agents). Then agents starting from cell i sample θ from the distribution $P(\theta; R, \nu) \sim \tilde{d}_i(\theta; R)^\nu$ with parameter $\nu \geq 0$ (Fig. 4a). We will refer to this modification of the EPR model as the Preferential Exploration and Preferential Return (PEPR) model (an alternative mechanism of preferential exploration has been proposed by Pappalardo et al.⁴¹; however, it im-

poses the gravity law¹², and thus a presumed aggregate behaviour, on the motion of the agents). Simulations (Fig. 4b-f) show that the PEPR model not only generates the distance-frequency scaling of the spectral flows with the correct scaling exponent; it also leads to the formation of clear spatial clusters which follow an area distribution that is quantitatively consistent with the data. Note that the exact spatial layout of the model clusters is different to the empirical data, since the current model setup ignores many complexities which likely influence the development of human settlements such as natural resources, rivers and topography. However, such factors can be integrated in future model extensions.

Prediction of origin-destination flows

Equation (1) implies that the magnitude of the entire distance-frequency spectrum of flows to any location can, in principle, be obtained by just knowing one single point on the universal scaling curve. This simplification opens up a wide range of possibilities for the prediction of various flow quantities between each pair of locations. As an example, for a given destination j the magnitude μ_j can be estimated from the population density, assuming that individuals return back home on a daily basis²⁵ which generates a local flow with minimum frequency $f_{\text{home}} \approx 1 \text{ day}^{-1}$. This leads to the approximation $\mu_j \approx \rho_{\text{pop}}(j)r_j^2 f_{\text{home}}$, where $\rho_{\text{pop}}(j)$ is the population density at location j and r_j is the distance to the boundary of the location (see derivation in Methods). Once the value of μ_j is established, it is straightforward to calculate the number of trips or the number of unique visitors from any origin location. These predictions are in remarkable agreement with the data (Fig. 5). Besides population density, other input quantities such as simple traffic counts are equally

well suited (especially for those locations where population density is not a good predictor, see Supplementary Information).

To put the accuracy of these predictions in relation to existing approaches, we compared them to those of the gravity model^{12,13} and the radiation model¹⁴, which currently are the most widely used mobility models for aggregate population flows²⁵ (Methods). These established approaches do not take into account the frequency component of the flows. Thus, the gravity model requires separate parameter calibrations for each specific flow quantity, so that knowing the number of *trips* does not allow to infer how many *unique individuals* are actually visiting a location over time and vice-versa. Similarly, since each individual may give rise to several trips to multiple locations, the radiation model can predict the number of trips but not the number of unique individuals who are visiting a location over time. This ignorance of the frequency spectrum may lead to biased conclusions regarding the spatial mixing of people with potentially far-reaching consequences, e.g., for understanding the spreading of infectious diseases. Our framework addresses this limitation. It is applicable in particular to fine-grained spatial scales (Fig. 5a, again using Back Bay West in Boston as an illustrative example) and it allows for the simultaneous prediction of both the number of trips *and* the number of individuals across the entire frequency spectrum without the need for model calibrations (Fig. 5b,c). Predictions of origin-destination flows in all world regions considered here empirically confirm the enhanced performance of our framework (Fig. 5d).

Discussion

Given the extensive literature on and detailed analyses of movement and transport in cities, it is surprising that the simple but powerful visitation law derived here had not yet been discovered. It states that the number of visitors to any location scales as the inverse square of both travel distance and visitation frequency and thus advances our understanding of human mobility by the frequency spectrum of flows. We have shown that the scaling relation is remarkably robust across different geographies, cultures and levels of development, and that it is consistent with our state-of-the-art understanding of the mobility patterns of individuals.

This new perspective on human mobility makes it possible to scrutinise long-standing conjectures in human geography and spatial economics. Indeed, the distance-frequency distribution of visits corroborates several key ideas behind the well-known central place theory (CPT)^{16,36} that, so far, have been difficult to test. For instance, our results support the existence of a nested hierarchy of locations (Fig. 1 and Fig. 3), in which higher-order centres with specialised functions (e.g., shopping centres, museums) – reflected in lower visitation frequencies – also embrace non-specialised functions of lower-order centres (e.g., groceries, restaurants) – reflected in higher visitation frequencies. Thereby, more specialised functions are associated not only with a lower visitation frequency but also with a larger service radius (i.e., people travel further). This is again supported by our data, showing that the average travel distance per visit is inversely proportional to the visitation frequency (Extended Data Fig. 9 and Supplementary Information for a more detailed discussion).

An interesting question here is how close the revealed visitation patterns are to the most efficient spatial configuration of the attracting locations, as postulated by CPT and other theories in human geography^{1,15}. To that end, we computed the Fermat-Torricelli-Weber⁴² metric used in spatial economy. The metric determines for each attracting location the potential reduction in the effective distance travelled by all its visitors when moving the location to another geographic position. Interestingly, we find that for most locations it is not possible to appreciably reduce the visitors' effective travel distance, showing that the current spatial configuration of the locations is close to the optimum in terms of transportation efficiency (Extended Data Fig. 10). While game theory shows that collective human behaviour is often non-rational and far from the socially desired outcome^{43,44}, this result suggest that, when it comes to travel effort, humans are able to achieve optimal group-level behaviour (see Supplementary Information for details).

From a practical view, we have shown that the discovered visitation law opens up new possibilities to accurately predict recurrent population flows of varying frequencies, offering immediate applications for traffic engineering, urban planning and the containment of epidemic diseases. In future work, these predictions can be further refined by establishing the detailed connection between the characteristics of a location and the frequencies of recurrent visits.

1. Batty, M. *The New Science of Cities* (MIT Press, 2013).
2. Barthelemy, M. *The Structure and Dynamics of Cities* (Cambridge University Press, 2016).
3. Louail, T. *et al.* Uncovering the spatial structure of mobility networks. *Nature Communications* **6**, 1–8 (2015).

4. Anderson, R. M., Anderson, B. & May, R. M. *Infectious Diseases of Humans: Dynamics and Control* (Oxford University Press, 1992).
5. Eubank, S. *et al.* Modelling disease outbreaks in realistic urban social networks. *Nature* **429**, 180–184 (2004).
6. Wesolowski, A. *et al.* Quantifying the impact of human mobility on malaria. *Science* **338**, 267–270 (2012).
7. Jia, J. S. *et al.* Population flow drives spatio-temporal distribution of COVID-19 in China. *Nature* **582**, 389–394 (2020).
8. Bettencourt, L. M. A. The origins of scaling in cities. *Science* **340**, 1438–1441 (2013).
9. Glaeser, E. L., Kallal, H. D., Scheinkman, J. A. & Shleifer, A. Growth in cities. *Journal of Political Economy* **100**, 1126–1152 (1992).
10. Fujita, M., Krugman, P. R. & Venables, A. J. *The Spatial Economy: Cities, Regions, and International Trade* (MIT Press, 1999).
11. Sveikauskas, L. The productivity of cities. *The Quarterly Journal of Economics* **89**, 393–413 (1975).
12. Zipf, G. K. The P1P2/D hypothesis: on the intercity movement of persons. *American Sociological Review* **11**, 677–686 (1946).
13. Erlander, S. & Stewart, N. F. *The Gravity Model in Transportation Analysis: Theory and Extensions* (CRC Press, 1990).

14. Simini, F., González, M. C., Maritan, A. & Barabási, A.-L. A universal model for mobility and migration patterns. *Nature* **484**, 96–100 (2012).
15. Zipf, G. K. *Human Behavior and the Principle of Least Effort* (Addison-Wesley, 1949).
16. Christaller, W. *Die zentralen Orte in Süddeutschland* (Gustav Fischer, 1933).
17. Pan, W., Ghoshal, G., Krumme, C., Cebrian, M. & Pentland, A. Urban characteristics attributable to density-driven tie formation. *Nature Communications* **4**, 1–7 (2013).
18. Schläpfer, M. *et al.* The scaling of human interactions with city size. *Journal of the Royal Society Interface* **11**, 20130789 (2014).
19. Li, R. *et al.* Simple spatial scaling rules behind complex cities. *Nature Communications* **8**, 1–7 (2017).
20. Anas, A., Arnott, R. & Small, K. A. Urban spatial structure. *Journal of Economic Literature* **36**, 1426–1464 (1998).
21. Henderson, V. & Thisse, J.-F. *Handbook of Regional and Urban Economics: Cities and Geography* (Elsevier, 2004).
22. Ewing, R. & Hamidi, S. Compactness versus sprawl: a review of recent evidence from the United States. *Journal of Planning Literature* **30**, 413–432 (2015).
23. Chang, S. *et al.* Mobility network models of COVID-19 explain inequities and inform reopening. *Nature* **589**, 82–87 (2021).

24. Axhausen, K. W. & Gärling, T. Activity-based approaches to travel analysis: conceptual frameworks, models, and research problems. *Transport Reviews* **12**, 323–341 (1992).
25. Barbosa, H. *et al.* Human mobility: models and applications. *Physics Reports* **734**, 1–74 (2018).
26. Stouffer, S. A. Intervening opportunities: a theory relating mobility and distance. *American Sociological Review* **5**, 845–867 (1940).
27. Noulas, A., Scellato, S., Lambiotte, R., Pontil, M. & Mascolo, C. A tale of many cities: universal patterns in human urban mobility. *PloS ONE* **7**, e37027 (2012).
28. Yan, X.-Y., Wang, W.-X., Gao, Z.-Y. & Lai, Y.-C. Universal model of individual and population mobility on diverse spatial scales. *Nature Communications* **8**, 1–9 (2017).
29. Mazzoli, M. *et al.* Field theory for recurrent mobility. *Nature Communications* **10**, 1–10 (2019).
30. Brockmann, D., Hufnagel, L. & Geisel, T. The scaling laws of human travel. *Nature* **439**, 462–465 (2006).
31. Gonzalez, M. C., Hidalgo, C. A. & Barabási, A.-L. Understanding individual human mobility patterns. *Nature* **453**, 779–782 (2008).
32. Song, C., Koren, T., Wang, P. & Barabási, A.-L. Modelling the scaling properties of human mobility. *Nature Physics* **6**, 818–823 (2010).

33. Alessandretti, L., Aslak, U. & Lehmann, S. The scales of human mobility. *Nature* **587**, 402–407 (2020).
34. Bertaud, A. *Order Without Design: How Markets Shape Cities* (MIT Press, 2018).
35. Louail, T. *et al.* From mobile phone data to the spatial structure of cities. *Scientific Reports* **4**, 5276 (2014).
36. Zhong, C. *et al.* Revealing centrality in the spatial structure of cities from human activity patterns. *Urban Studies* **54**, 437–455 (2017).
37. Rozenfeld, H. D. *et al.* Laws of population growth. *Proceedings of the National Academy of Sciences* **105**, 18702–18707 (2008).
38. Cao, W., Dong, L., Wu, L. & Liu, Y. Quantifying urban areas with multi-source data based on percolation theory. *Remote Sensing of Environment* **241**, 111730 (2020).
39. Batty, M. The size, scale, and shape of cities. *Science* **319**, 769–771 (2008).
40. Rozenfeld, H. D., Rybski, D., Gabaix, X. & Makse, H. A. The area and population of cities: new insights from a different perspective on cities. *American Economic Review* **101**, 2205–2225 (2011).
41. Pappalardo, L. *et al.* Returners and explorers dichotomy in human mobility. *Nature Communications* **6**, 1–8 (2015).
42. Weber, A. & Friedrich, C. J. *Alfred Weber's Theory of the Location of Industries* (The University of Chicago Press, 1929).

43. Kreps, D. M. *Game Theory and Economic Modelling* (Oxford University Press, 1990).
44. Myerson, R. B. *Game Theory* (Harvard University Press, 2013).
45. Blondel, V. D., Decuyper, A. & Krings, G. A survey of results on mobile phone datasets analysis. *EPJ Data Science* **4**, 10 (2015).
46. Calabrese, F., Diao, M., Di Lorenzo, G., Ferreira Jr, J. & Ratti, C. Understanding individual mobility patterns from urban sensing data: a mobile phone trace example. *Transportation Research Part C: Emerging Technologies* **26**, 301–313 (2013).
47. de Montjoye, Y.-A., Smoreda, Z., Trinquart, R., Ziemlicki, C. & Blondel, V. D. D4D-Senegal: the second mobile phone data for development challenge. Preprint at <https://arxiv.org/abs/1407.4885> (2014).
48. Blondel, V. D. *et al.* Data for development: the D4D challenge on mobile phone data. Preprint at <https://arxiv.org/abs/1210.0137> (2012).
49. Jiang, S. *et al.* The TimeGeo modeling framework for urban mobility without travel surveys. *Proceedings of the National Academy of Sciences* **113**, E5370–E5378 (2016).
50. Song, C., Qu, Z., Blumm, N. & Barabási, A.-L. Limits of predictability in human mobility. *Science* **327**, 1018–1021 (2010).
51. Wilson, A. G. The use of entropy maximising models in the theory of trip distribution, mode split and route split. *Journal of Transport Economics and Policy* 108–126 (1969).

52. Masucci, A. P., Serras, J., Johansson, A. & Batty, M. Gravity versus radiation models: on the importance of scale and heterogeneity in commuting flows. *Physical Review E* **88**, 022812 (2013).

Acknowledgements: We thank Luís M.A. Bettencourt, Roberta Sinatra, Pieter Herthogs, Guangyu Du, Youguo Qin and Yu Liu for helpful discussions, Wenpu Cao for assistance to perform the CCA analysis and Sebastian Grauwin for providing the Matlab code for the radiation model. We acknowledge Airsage, ORANGE / SONATEL and Singtel for providing the data. This work was supported by the National Science Foundation, the AT&T Foundation, the MIT SMART program, the MIT CCES program, Audi Volkswagen, BBVA, Ericsson, Ferrovial, GE, the MIT Senseable City Lab Consortium, the John Templeton Foundation (grant no. 15705), the Eugene and Clare Thaw Charitable Trust, the US Army Research Office Minerva Programme (grant no. W911NF-12-1-0097), the Singapore National Research Foundation (FI 370074016) and the National Natural Science Foundation of China (grant no. 41801299).

Author contributions: G.B.W., C.R., M.Sc., L.D., K.O. and P.S. designed the research. L.D., M.Sc., K.O. and M.V. processed and analysed the data. G.B.W. and M.Sc. identified the data collapse to a single, universal curve. K.O., L.D., S.A. and P.S. developed the PEPR model. H.S., M.Sc. and G.B.W. developed the theoretical argument. M.V. and P.S. tested the Fermat-Toricelli-Weber metric. L.D., M.Sc., K.O., M.Sz., P.S., G.B.W and C.R. wrote the paper. All authors discussed the results and reviewed the manuscript.

Competing interests: The authors have no competing financial interests.

Data availability: Raw mobility data are not publicly available to preserve privacy. Grid cell level data to reproduce the findings of this study can be requested from the corresponding author.

Code availability: The code to replicate this research can be requested from the corresponding author (<https://github.com/leiii/VisitationLaw>).

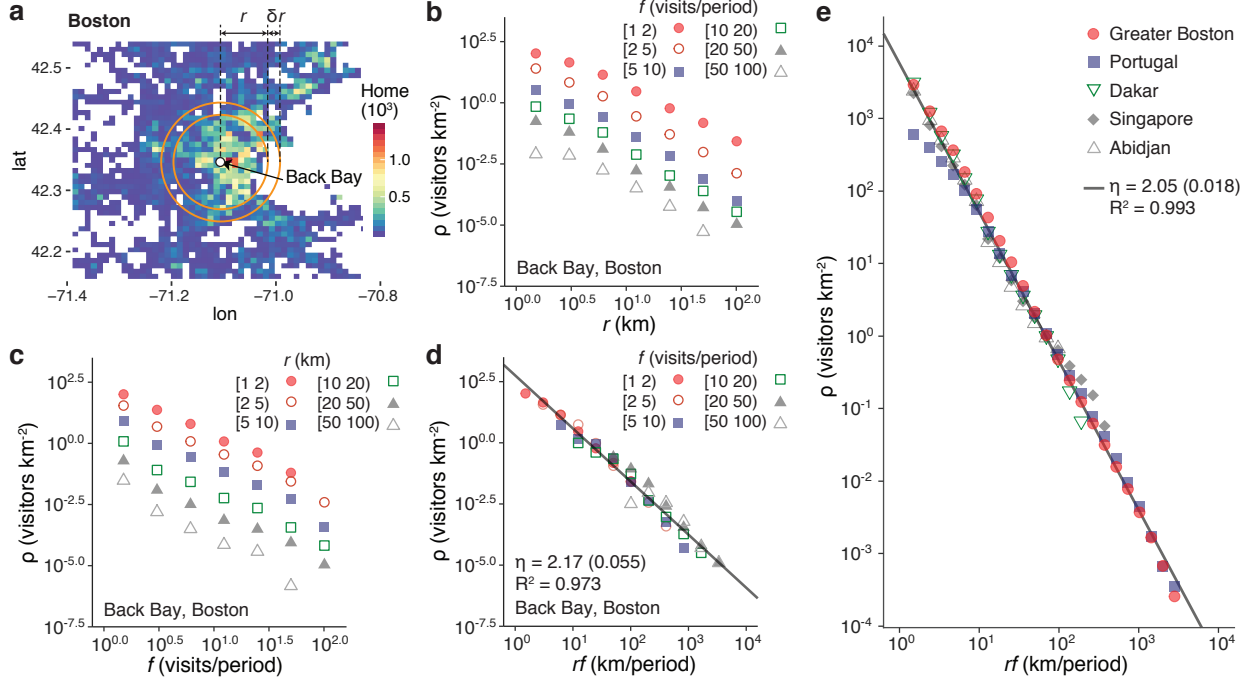


Figure 1: The universal distance-frequency distribution of population flows. **a**, For each location, we count the number of visitors who are living at a distance $[r, r + \delta r]$ away and are visiting with frequency f . The map colours indicate the population density derived from the mobile phone data (users per grid cell). **b**, For a fixed frequency f , the visitor flow to a specific location, $\rho_i(r, f)$, decreases with increasing distance r . **c**, When keeping the distance r fixed, the flow decreases similarly with increasing frequency f . **d**, Rescaled values collapse onto a single curve, making the flows dependent only on the single variable rf . The entire distance-frequency distribution is very well described by a power law of the form $\rho_i(r, f) = \mu_i/(rf)^\eta$, with exponent $\eta \approx 2$ (η is the slope of the best-fit line by the least squares method; standard error in parentheses). **e**, Rescaled flows across all studied regions, demonstrating that the same scaling relation holds for radically different urban regions worldwide. Symbols are average values across all locations in each region. To visually compare the different world regions, the shown curves were superimposed by normalising the distance-frequency distribution of each individual location.

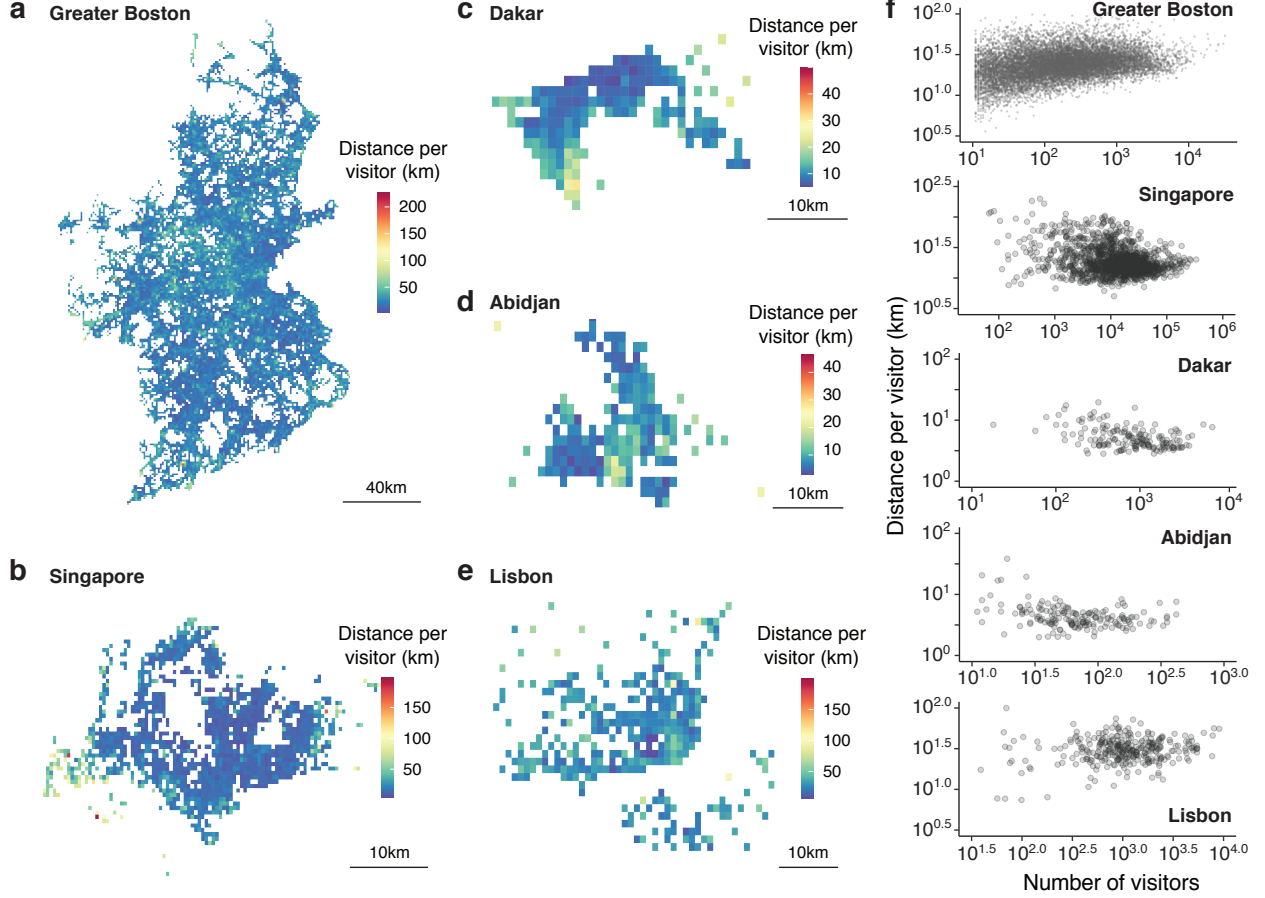


Figure 2: Constant effective travel distance per visitor. a-f, The average effective distance, $\langle d \rangle_i$, covered by an individual over time to visit a given location i is largely invariant across space and independent of the attractiveness of the location (in terms of number of visitors). The R^2 values of the linear regression between the number of visitors and average distance per visitor, as shown in the scatter plots (panel f), are very small (Greater Boston, $R^2 = 0.0115$; Singapore, $R^2 = 0.0298$; Dakar, $R^2 < 0.001$; Abidjan, $R^2 < 0.001$; Lisbon, $R^2 = 0.001$). Notice that there are some ‘anomalous’ locations that are associated with larger effective travel distances. In the majority of cases, these locations correspond to ports (e.g., Singapore and Dakar) or tourism attractions (Lisbon), thus having an intrinsic reason to attract visitors from particularly far away.

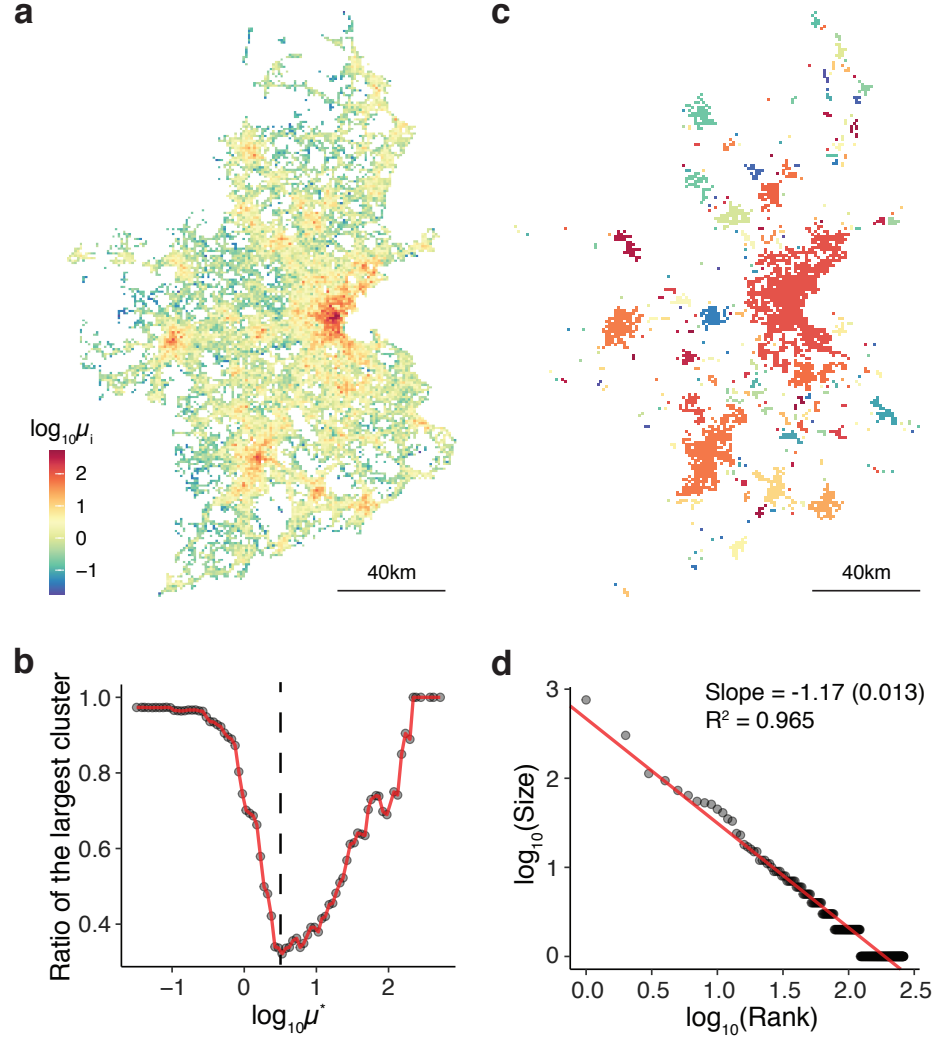


Figure 3: Spatial structure of the location-specific attractiveness. **a**, Geographic distribution of the attractiveness values μ_i across the Greater Boston area. **b**, Area ratio of the largest spatial cluster to all spatial clusters versus the minimum attractiveness threshold μ^* as derived through the City Clustering Algorithm (CCA)^{37,38}. For very small values of μ^* the entire geographic area is merged into one single cluster (resulting in an area ratio of ≈ 1). Conversely, for very large values of μ^* , only one cluster (Boston downtown) would exist (again resulting in a ratio of ≈ 1). **c**, Detected clusters at the critical value of $\mu^* \approx 10^{0.5}$, where the area ratio of the largest cluster is minimised (vertical dashed line in panel **b**). Distinct clusters are represented by different colours. **d**, Rank-size distribution at the the critical value of μ^* . Consistent with Zipf's law, the data are well approximated by a power law with exponent $\zeta = -1.17$.

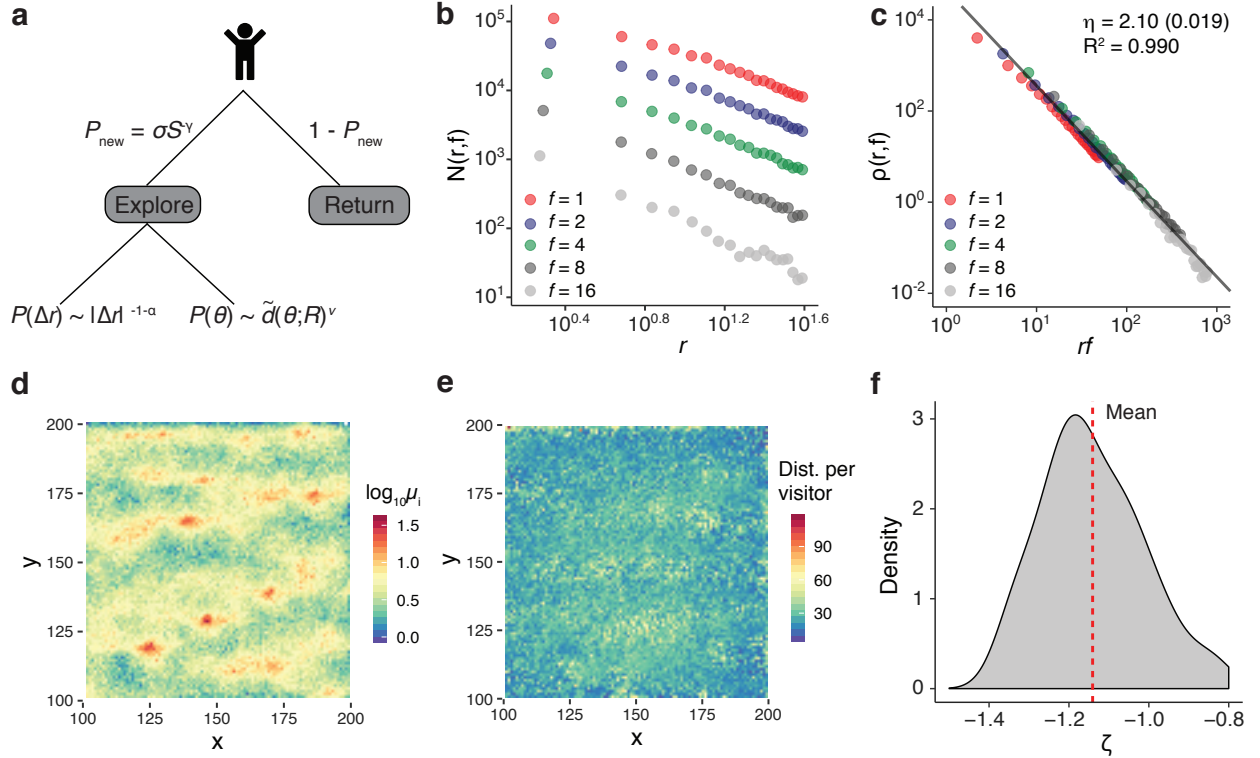


Figure 4: Microscopic model of spectral population flows. **a**, Schematics of the Preferential Exploration and Preferential Return (PEPR) model. At each time step, an individual (agent) decides to explore a previously unvisited location with probability P_{new} . The radial distance Δr and direction θ of this displacement are drawn from random distributions that capture the characteristic jump-size distribution of human trajectories and the propensity to explore popular areas. With probability $1 - P_{\text{new}}$ the agent returns to a previously visited location. **b-f**, Results for $n_a = 10^5$ agents on a regular square grid (with parameters $\alpha = 0.55$, $\sigma = 0.6$, $\gamma = 0.21$ according to existing measurements³² and $R = 10$, $\nu = 4$ determined experimentally, see Methods). Panels **b,c** show the spectral flows, obtained via numerical simulation of the model and averaged over all analysed grid cells, exhibiting the scaling properties of the empirically observed population flows; i.e., they obey equation (1) and scale as the inverse square of travel distance and visitation frequency. Consistent with the empirical results, the model gives rise to a spatial clustering of those cells that attract a high number of individuals (**d**), while the effective travel distance per agent and time unit remains spatially invariant (**e**). The area distribution of the spatial clusters follows Zipf's law (derived through the application of the CCA with threshold $\mu^* = 10$ to a total of 50 model realisations, leading to a power-law scaling with exponent $\zeta = -1.14 \pm 0.13$ (s.d.)), which is again in agreement with the data (**f**).

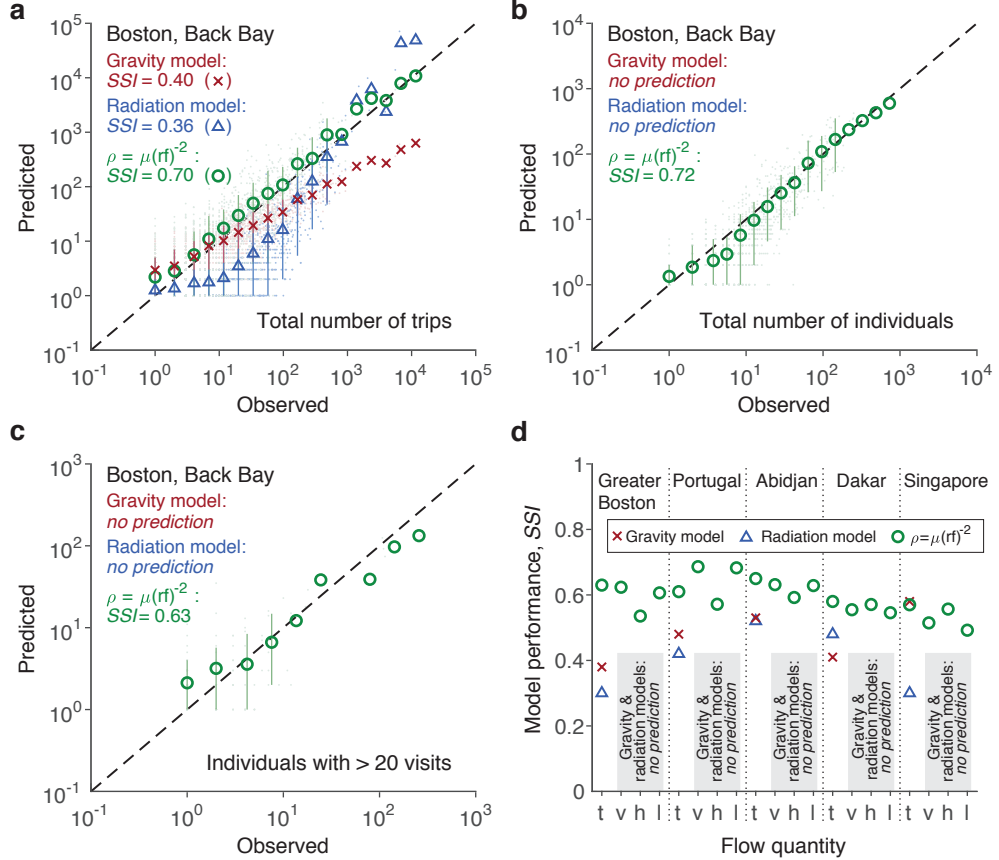


Figure 5: Predicting the flows between individual locations. **a**, Predictions for the observed trips to Back Bay, Boston, derived from the gravity law and the radiation model compared to predictions based on the rf -scaling framework. Symbols are mean values for each bin and lines are the 0.1-0.9 quantiles. The dashed line corresponds to a perfect agreement between the observed values and the predictions, clearly showing that the rf -scaling framework systematically outperforms the existing models. The performance of each model is further quantified based on the Sørensen-Dice similarity index (SSI), with $SSI = 1$ if there is a perfect match and $SSI = 0$ if there is no match at all (see Methods). **b**, Number of unique visitors. The fitting parameters of the gravity law from the number of trips (**a**) do not allow to predict the number of individuals. The radiation model does not provide a prediction of the number of visitors either, because it assigns only one destination location to each individual. It is therefore unable to explicitly consider the fact that an individual may visit several different locations. **c**, Number of high-frequency visitors. **d**, Systematic comparison over all considered locations in the studied world regions for number of trips (t), number of visitors (v), number of high-frequency visitors (h) and low-frequency visitors (l). The gravity model (calibrated for t) and the radiation model are unable to predict v , h or l . The rf -scaling overcomes this limitation.

Methods

Data description. For the empirical analysis, we make use of five mobile phone data sets that differ strongly in terms of the geographic region, the socioeconomic and infrastructural setting and in terms of the underlying data collection method, thus providing several safeguards that variations of these factors do not influence the results. These data sets are from Greater Boston, Portugal, Senegal, Ivory Coast and Singapore. Together, our data sets contain more than 3 billion time-stamped location records of more than 8 million anonymised users. Generally, mobile phone location records are considered as the most comprehensive type of data for the study of population-wide movement patterns^{25,45}.

The data set for the Greater Boston area contains ≈ 1 billion location records from ≈ 2 million anonymised mobile phone users during 4 months in 2009 (July-October)⁴⁶. Each record consists of an anonymised ID of the corresponding user, latitude, longitude and a time stamp. These records were generated each time a user connected to the mobile phone network (through calls, text messages (SMS) and Internet connections). The latitude and longitude of each record were approximated by the data provider through cell tower triangulation⁴⁶. As a result, the records have a precision of $\approx 220\text{m}$ and thus have a much higher spatial resolution than tower-based records (see Supplementary Information for the sampling statistics).

The data set covering Portugal consists of ≈ 440 million call detail records (CDRs) from ≈ 2 million anonymised users¹⁸. The CDRs are restricted to voice calls and were collected by a single telecom provider over a period of 8 months in the years 2006 and 2007. Each CDR consists of

the anonymised IDs of the two connected individuals, the call duration, the date and time of the call initiation, as well as the IDs of the two mobile phone towers routing the call at its initiation. In total, the data set contains 6,511 mobile phone towers together with their geographic location (latitude and longitude). Due to the sparsity of the mobile phone towers in rural areas, the statistical analysis of the influx is limited to those grid cells that are located within the metropolitan areas (Larger Urban Zones) of Lisbon, Porto and Braga (Supplementary Information section I).

The data set of Senegal is based on anonymised CDRs provided by the telecom provider Sonatel and the Orange Group within the context of the Data for Development (D4D) Senegal Challenge⁴⁷. It covers the year 2013 and is divided into 25 individual two-week periods. Each period contains ≈ 44 million tower-based location records of $\approx 300,000$ randomly sampled and anonymised users. The temporal resolution is 10 min, while the spatial resolution is given by the provider's 1,666 mobile phone towers distributed over the country. The statistical analysis of the influx is limited to the region of Dakar (Supplementary Information section I).

The data set of Ivory Coast is based on anonymised CDRs provided by the D4D Ivory Coast Challenge⁴⁸. It covers the time between December 1, 2011 and April 28, 2012 and is split into two-week periods. Each period contains individual trajectories for 50,000 randomly sampled users. The spatial resolution is given by the provider's 1,231 mobile phone towers. The statistical analysis of the influx is limited to the region of Abidjan (Supplementary Information section I).

The data set of Singapore consists of ≈ 4 million anonymised users of Singapore's largest telecom company. The data were collected during a two-month period from mid-March to mid-

May 2011 for billing purposes. A time-stamped record was produced when a call was initiated or received (both at the beginning and the end of the call), an SMS was sent or received, or when the mobile phone connected to the Internet. Each record contains the ID of the mobile phone tower routing the activity. In total, there are 5,587 mobile phone towers for which the geographic location was provided.

Data preprocessing. In a first step, each study area was partitioned into a regular grid with equally sized square cells of size $s_0 \times s_0$. We used $s_0 = 500$ m for Greater Boston and Singapore and $s_0 = 1$ km for Portugal, Senegal and Ivory Coast (Supplementary Fig. S2). We additionally tested the robustness of our results against variations in the cell size (Supplementary Information section II). Subsequently, for each grid cell, we identified those users who visited the location with a given frequency. To do so, we imposed a minimum stay time, τ , during which a user had to stay inside a given cell in order to be counted. This removed those users who only travelled through a given grid cell without engaging in some form of activity⁴⁹. If not stated otherwise, a minimum stay time of $\tau = 1$ h was used, but our findings are robust against variations in the specific value (Supplementary Information section II).

Using a temporal resolution of one day, the visitation frequency f corresponds to the number of distinct days during which a user visited a given grid cell per observation period T , with $T = 4$ months for Greater Boston, $T = 8$ months for Portugal, $T = 2$ weeks for Senegal and Ivory Coast, and $T = 2$ months for Singapore. The statistical analysis of the distance-frequency distribution is then based on those grid cells that during T attract at least 10 visitors from neighbouring

grid cells (whereas we considered the flows originating from all cells, including those that have less than 10 visitors).

The home location of each mobile phone user was determined using a standard procedure⁴⁶. Specifically, for each user the home location was assumed to be the cell with the largest number of nights (8pm-7am) during which she/he visited that cell (Supplementary Fig. S2). In line with previous work⁵⁰, we only considered regularly active users that visited their home location, on average, at least during one night per week ($f_{\text{home,data}} = 1 \text{ week}^{-1}$) for the case of Greater Boston, Senegal, Ivory Coast and Singapore and at least during one night per two-week period ($f_{\text{home,data}} = 0.5 \text{ week}^{-1}$) for the case of Portugal (due to the lower number of location records).

Effective travel distance per visitor. For a given location i , the effective travel distance per visitor during the observation period is $\langle d \rangle_i = d_i^{\text{tot}} / N_i^{\text{tot}}$, where d_i^{tot} is the effective distance travelled by all visitors (N_i^{tot}) during the time period T . Thus, $\langle d \rangle_i = \frac{\sum_f \iint r f T \rho_i(r,f) r dr d\varphi}{\sum_f \iint \rho_i(r,f) r dr d\varphi} = \frac{\sum_f \int T(rf)^{-1} r dr}{\sum_f \int (rf)^{-2} r dr}$ (where φ is the angle of the influx), which does not depend on μ_i .

PEPR model and simulation procedure. The probability that an agent chooses to explore a previously unvisited location is $P_{\text{new}} = \sigma S^{-\gamma}$, where S is the number of locations the agent visited so far. The parameter values $\sigma = 0.6$ and $\gamma = 0.21$ were taken from Song et al.³², so that P_{new} decreases as the agent visits more and more locations. With complementary probability $1 - P_{\text{new}}$, the agent returns to one of the previously visited locations. The agent selects this location with a probability that is proportional to the number of the agent's previous visits to that location.

Numerical simulations were performed for a population of $n_a = 10^5$ agents moving on a regular square grid of 300×300 cells that represent possible locations. The home locations of these agents correspond to their initial position (at time $t = 0$) assigned uniformly at random across an inner grid of 100×100 cells. Analysis was confined to the inner grid only; the purpose of the outer 300×300 grid was to eliminate boundary effects. If an agent jumped outside the 300×300 grid, his/her trajectory was stopped. Simulations followed a discrete-time scheme, updating the position of a given agent after every time step $\Delta t = 1$ (for simplicity, the duration of the visits does not follow a waiting-time distribution as in the original EPR model³²). Agents were simulated ‘one at a time’: the first agent executes his/her trajectory from $t = 0, \dots, 10^3$, then the second agent begins his/her trajectory and so on. After $T = 10^3$ an approximate steady state was achieved in which the motion of each agent becomes dominated by his/her most visited locations and the mean displacement from his/her initial position saturates (or the agent has jumped outside the grid). Simulation with different grid sizes and simulation times did not appreciably alter the results. Finally, the parameter values for the preferential exploration mechanism (R, ν) were found by strobining over a grid in parameter space and selecting those values that led to a cluster size distribution following Zipf’s law (the distance-frequency scaling is not sensitive against changes in R and ν).

Estimating origin-destination flows from population density. The use of population density for estimating the flows to a location j is based on three assumptions: (1) Due to the daily rhythms of human activity²⁵, individuals return to their home location with a minimum frequency of $f_{\text{home}} \approx 1 \text{ day}^{-1}$. (2) The population density $\rho_{\text{pop}}(j)$ within the location’s area of radius r_j is equal to

the population density at its boundary. (3) While any distance that is sufficiently large to be of practical relevance (more than a few tens of meters) implies a substantial reduction in the number of visitors, individuals who are theoretically living on the boundary visit j with approximately the same minimum frequency as those living inside the area of j (Extended Data Fig. 8). Therefore, a frequency $f \geq f_{\min} \approx f_{\text{home}}$ can be associated to them (since the approach is continuous, moving just a few meters away from the boundary already results in individuals visiting less than once per day; i.e., $f_{\min} < f_{\text{home}}$). Under these assumptions, $\rho_{\text{pop}}(j)$ is deduced from the distribution $\{\rho_j(r_j, f)\}_{f \geq f_{\text{home}}}$ of individuals living on the boundary,

$$\rho_{\text{pop}}(j) \approx \int_{f_{\text{home}}}^{\infty} \rho_j(r_j, f) df = \frac{\mu_j}{r_j^2} \frac{1}{f_{\text{home}}}. \quad (2)$$

Consequently, the magnitude of the flows is approximated as $\mu_j \approx \rho_{\text{pop}}(j) r_j^2 f_{\text{home}}$. Because the empirical data are based on mobile phone records that do not cover every visit, the pre-set values $f_{\text{home,data}}$ (see Methods section ‘Data pre-processing’), are used for f_{home} (if the location recordings were complete, the natural choice would be $f_{\text{home}} \approx 1 \text{ day}^{-1}$).

The average daily number of trips of those individuals who live at an origin i and visit destination j is then $V_{ij} \approx \mathcal{A}_i \int_{f_{\min}}^{f_{\max}} f \rho_j df = \mu_j \mathcal{A}_i / r_{ij}^2 \ln(f_{\max}/f_{\min})$ with \mathcal{A}_i being the area of the origin location and r_{ij} being the distance between the origin and the destination. The main text (Fig. 5) reports the total number of trips, which also includes individuals living at j and returning home and is given as $V_{ij}^{\text{tot}} = V_{ji}^{\text{tot}} = (\mu_j \mathcal{A}_i + \mu_i \mathcal{A}_j) / r_{ij}^2 \ln(f_{\max}/f_{\min})$. The frequency limits can either be set according to the objective of the study (e.g., if the focus is on high-frequency visitors)

or, if all types of trips are to be included, they can be set as $f_{\min} = 1/T$, where $T \gg 1$ day is the observation period, and $f_{\max} = 1 \text{ day}^{-1}$ (for $r \gg r_j$). Because of the logarithmic form, even a large error in the estimation of the frequency limits does not appreciably affect V_{ij}^{tot} . The number of unique visitors, $Q_{ij} \approx \mathcal{A}_i \int \rho_j \, df$, is obtained in the same manner.

Gravity and radiation models. Gravity models are defined as $V_{ij} = Gm_i m_j / g(r_{ij})$, where V_{ij} is the number of trips (or number of commuters) from location i to location j , G is a constant, m_i and m_j represent key local attributes, and $g(r_{ij})$ describes the distance dependence of population flows^{12,25,51}. The distance-decay function g typically corresponds to a power-law or an exponential function. In the main text (Fig. 5), the (unconstrained) power-law form of the gravity model was used. It is defined as $V_{ij} = GP_i^a P_j^b / r_{ij}^c$, where P_i and P_j are the resident populations of cell i and cell j , respectively, and the model parameters G , a , b and c were determined by regression analysis. We additionally tested the exponential form of the distance dependence. In all regions, the model performance was substantially worse than that of the power-law form.

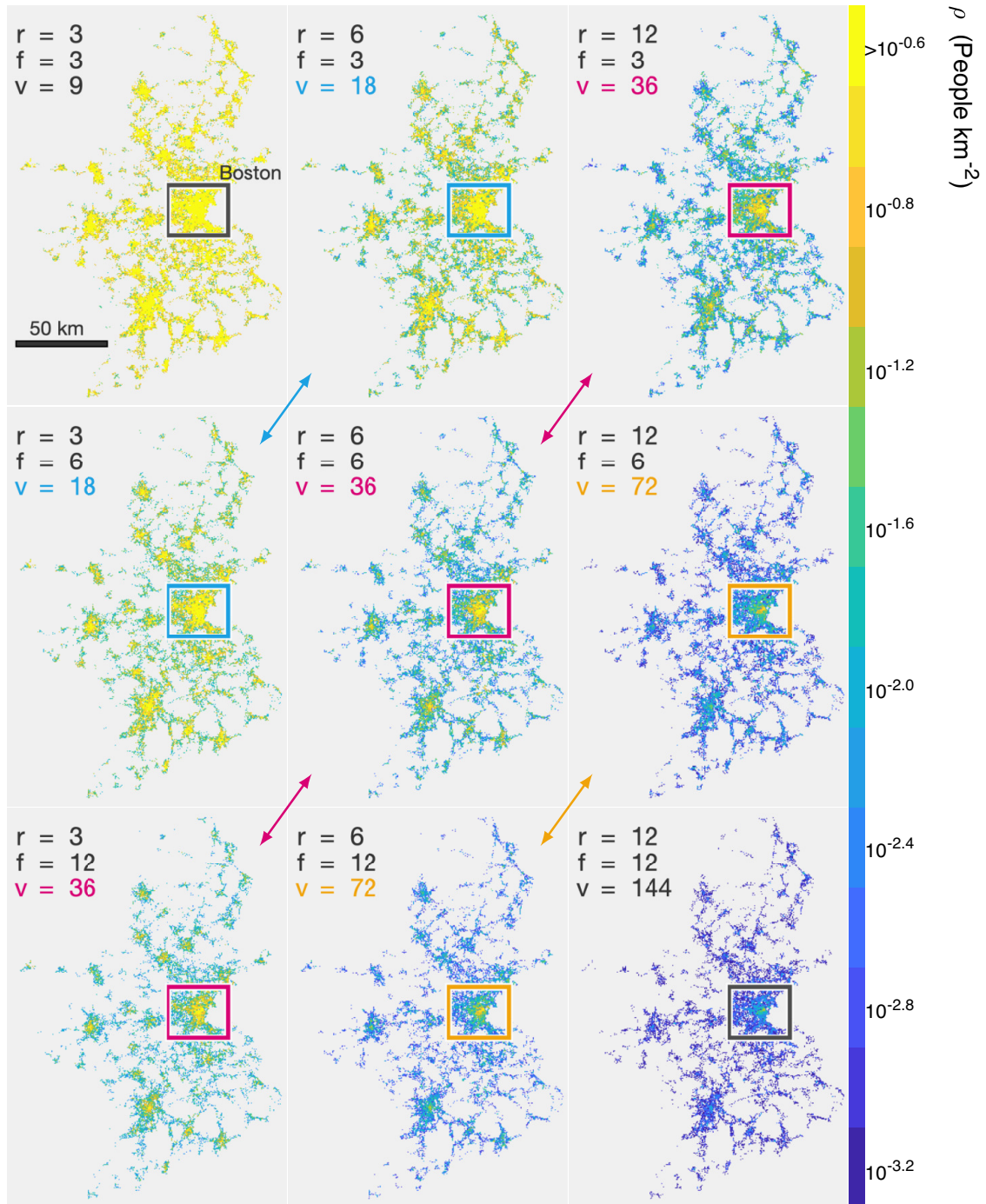
The radiation model¹⁴ is defined as $V_{ij} = V_i m_i m_j / [(m_i + s_{ij})(m_i + m_j + s_{ij})]$, where V_i is the number of trips (or number of commuters) per time starting from location i , m_i and m_j are the number of opportunities at the origin and at the destination, respectively, and s_{ij} is the number of opportunities within a circle of radius r_{ij} centred in i . In the main text, the standard form was used, which takes the population size of each grid cell as a proxy for the number of opportunities¹⁴.

To compare the performance of different mobility models, we applied the conventional performance index⁵², which is based on the Sørensen-Dice similarity index (SSI) in ecology. For each

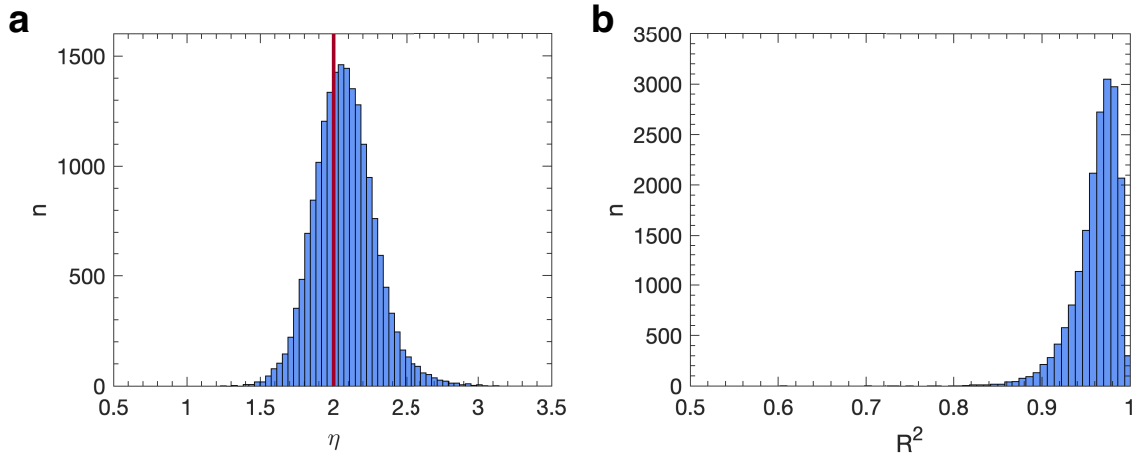
model, it quantifies the similarity between the predicted number of trips and the data as

$$\text{SSI} \equiv 2 \sum_{i,j} \min(V_{ij}^{\text{model}}, V_{ij}^{\text{data}}) / (\sum_{i,j} V_{ij}^{\text{model}} + \sum_{i,j} V_{ij}^{\text{data}}). \quad (3)$$

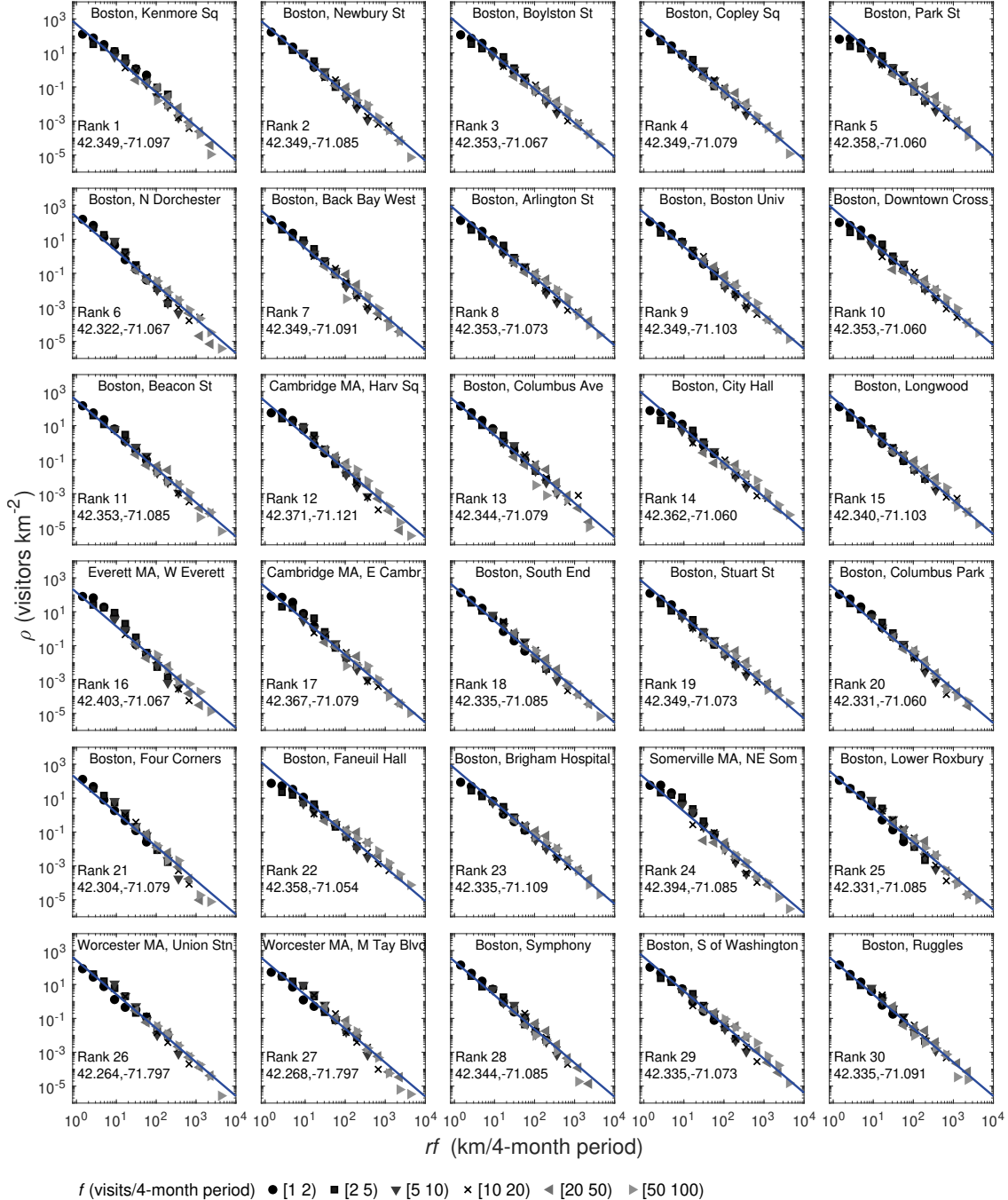
The coefficient takes values between 0, when no agreement is found, and 1, when there is a perfect match between the model and the data. Only flows originating from cells with a minimum user population of 25 individuals were considered in Fig. 5. The frequency threshold used to distinguish between low- and high-frequency visitors (Fig. 5d) was set to 5,2,4 visits per month for Boston, Portugal and Singapore, respectively, and to 2 visits per week for Dakar and Abidjan (roughly following the sampling frequency of the underlying data).



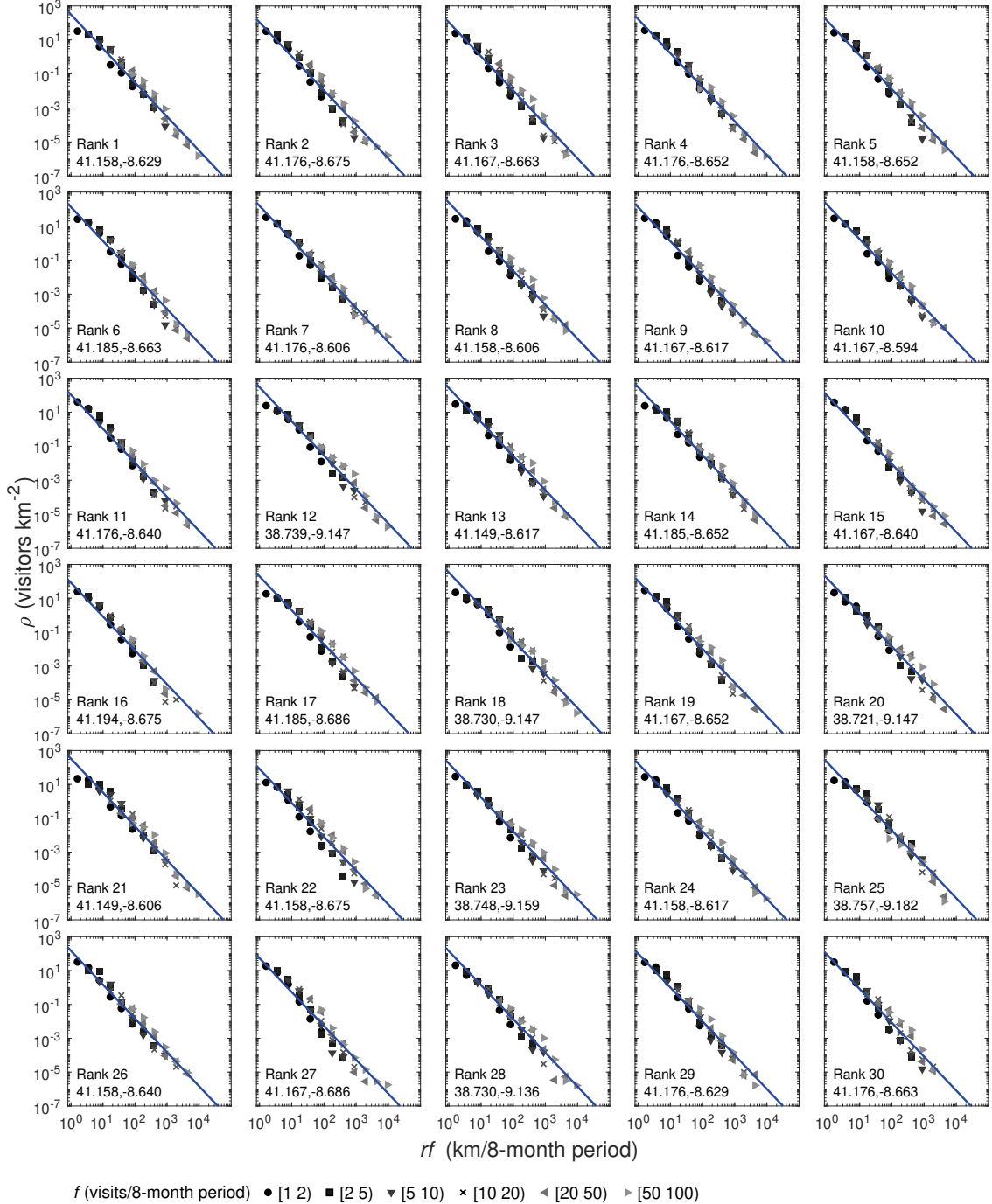
Extended Data Fig. 1 | The spatio-temporal structure of movement in cities. Panels show visitor influx maps for Greater Boston for different parameters (r, f). The colour of each grid cell ($500\text{m} \times 500\text{m}$) indicates the value of the spectral flow ρ . Remarkably, visitor influx maps for the same quantity $v = rf$ are nearly identical, as is clear from viewing along the diagonals indicated by the coloured arrows in the figure. Hence, doubling the visitation frequency f (from top row to bottom row) results in the same quantitative decrease of the influx as doubling the travel distance r (from left column to right column).



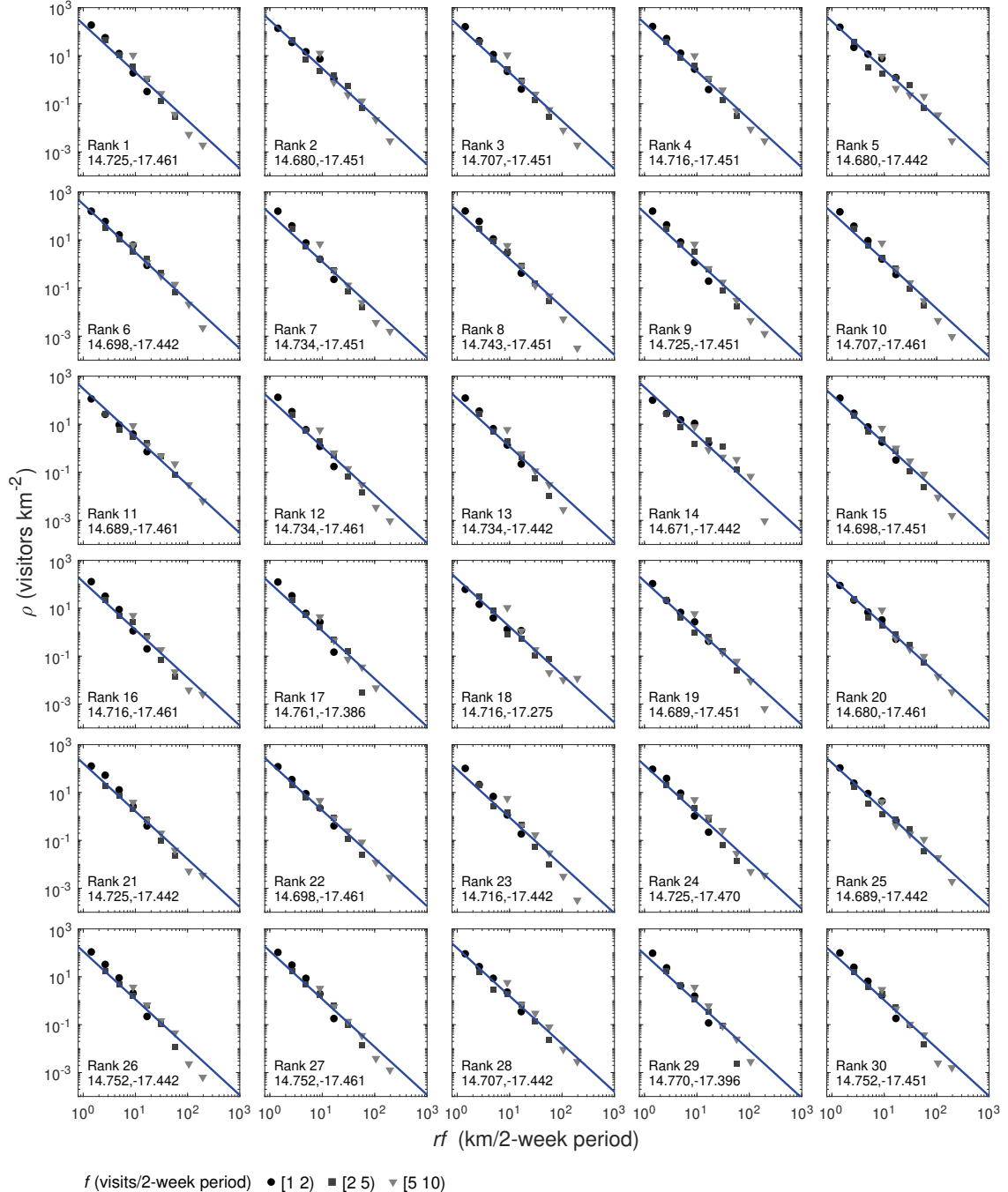
Extended Data Fig. 2 | Empirical power law exponents of the distance-frequency distribution. **a**, Histogram of the exponents for all locations in the Greater Boston area. The values were determined using ordinary least squares minimisation to a linear relation of the logarithmically transformed variables. The red line shows $\eta = 2$, consistent with our theoretical argument. **b**, Corresponding histogram of the R^2 -values.



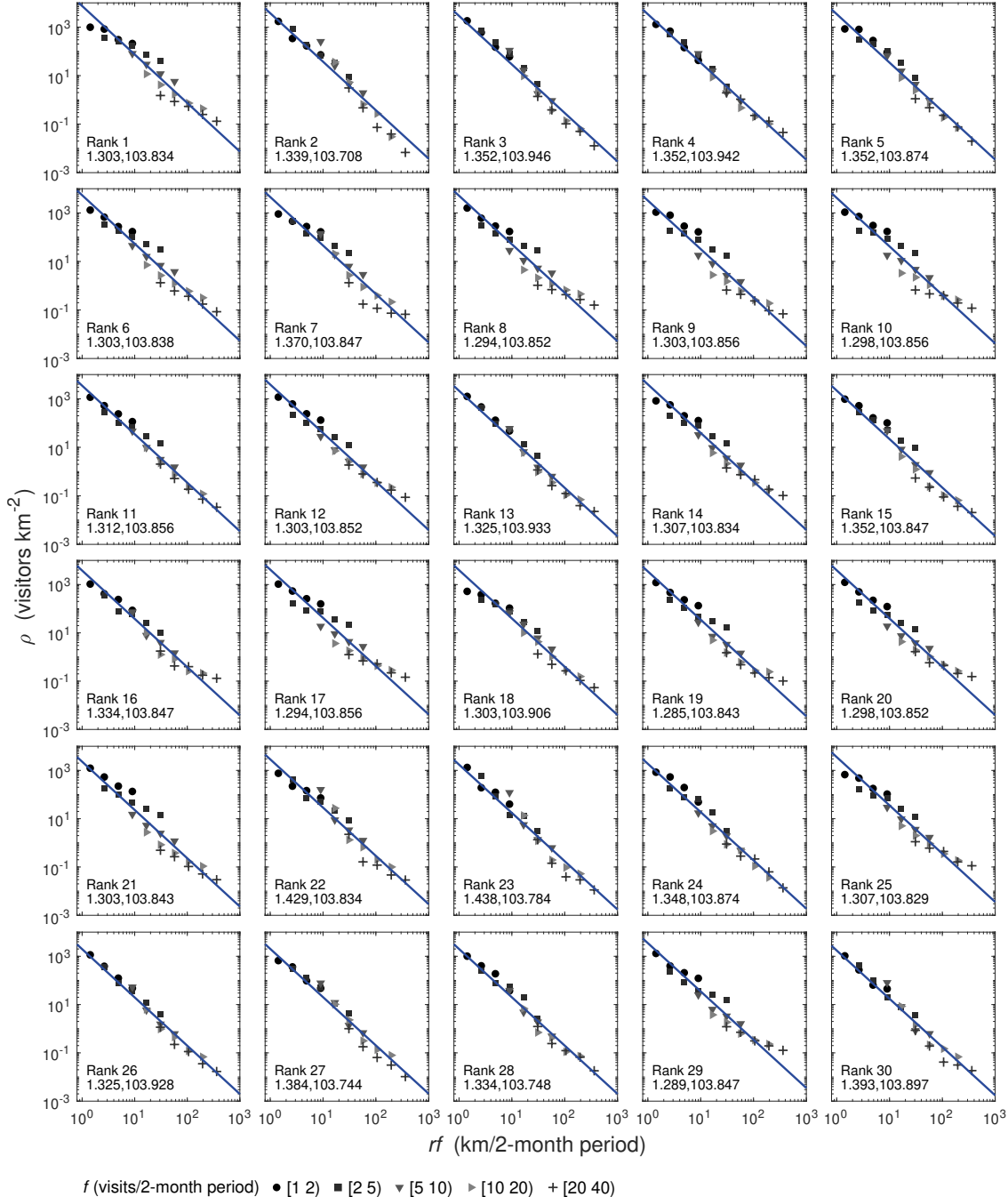
Extended Data Fig. 3 | Universality of the scaling relation $\rho \propto (rf)^{-2}$ across Greater Boston. The panels depict the data for individual locations (500m \times 500m grid cells), ranked according to the total number of visitors from neighbouring cells. Shown are locations of rank 1-30 (from top left to bottom right). The geographic coordinates of each location (latitude and longitude of the centre point of the grid cell) are indicated. The straight lines denote the inverse square of rf (slope = -2), consistent with our theoretical argument.



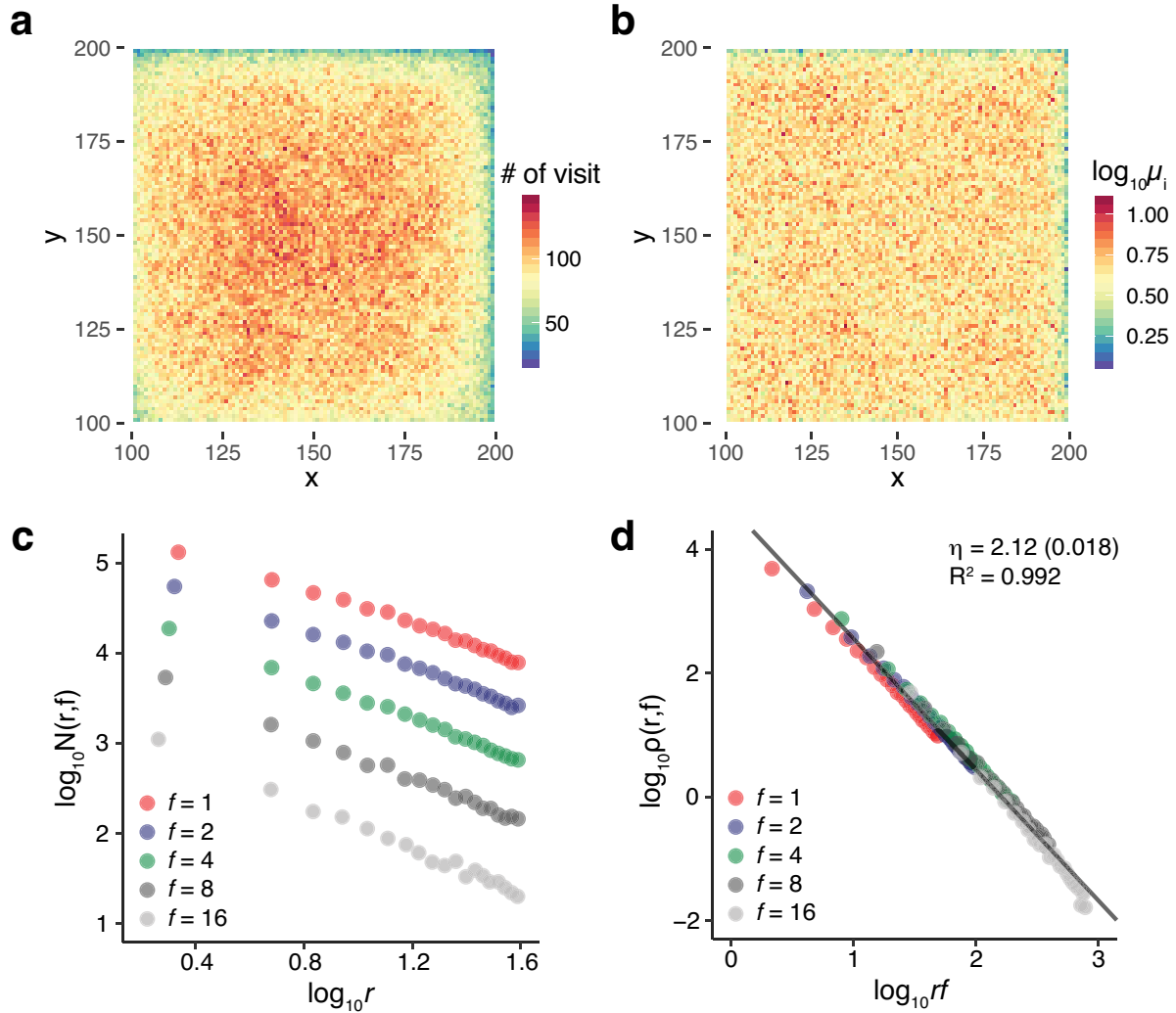
Extended Data Fig. 4 | Universality of the scaling relation $\rho \propto (rf)^{-2}$ across Portugal. The panels depict the data for individual locations ($1 \text{ km} \times 1 \text{ km}$ grid cells), ranked according to the total number of visitors from neighbouring cells. Shown are locations of rank 1-30 (from top left to bottom right). The geographic coordinates of each location (latitude and longitude of the centre point of the grid cell) are indicated. The straight lines denote the inverse square of rf (slope = -2), consistent with our theoretical argument.



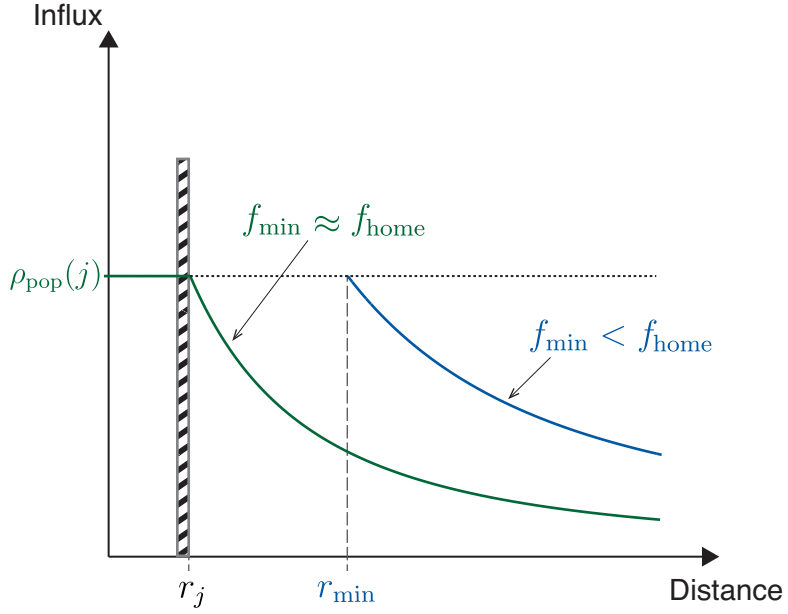
Extended Data Fig. 5 | Universality of the scaling relation $\rho \propto (rf)^{-2}$ across Dakar. The panels depict the data for individual locations (1 km \times 1 km grid cells), ranked according to the total number of visitors from neighbouring cells. Shown are locations of rank 1–30 (from top left to bottom right). The geographic coordinates of each location (latitude and longitude of the centre point of the grid cell) are indicated. The straight lines denote the inverse square of rf (slope = -2), consistent with our theoretical argument.



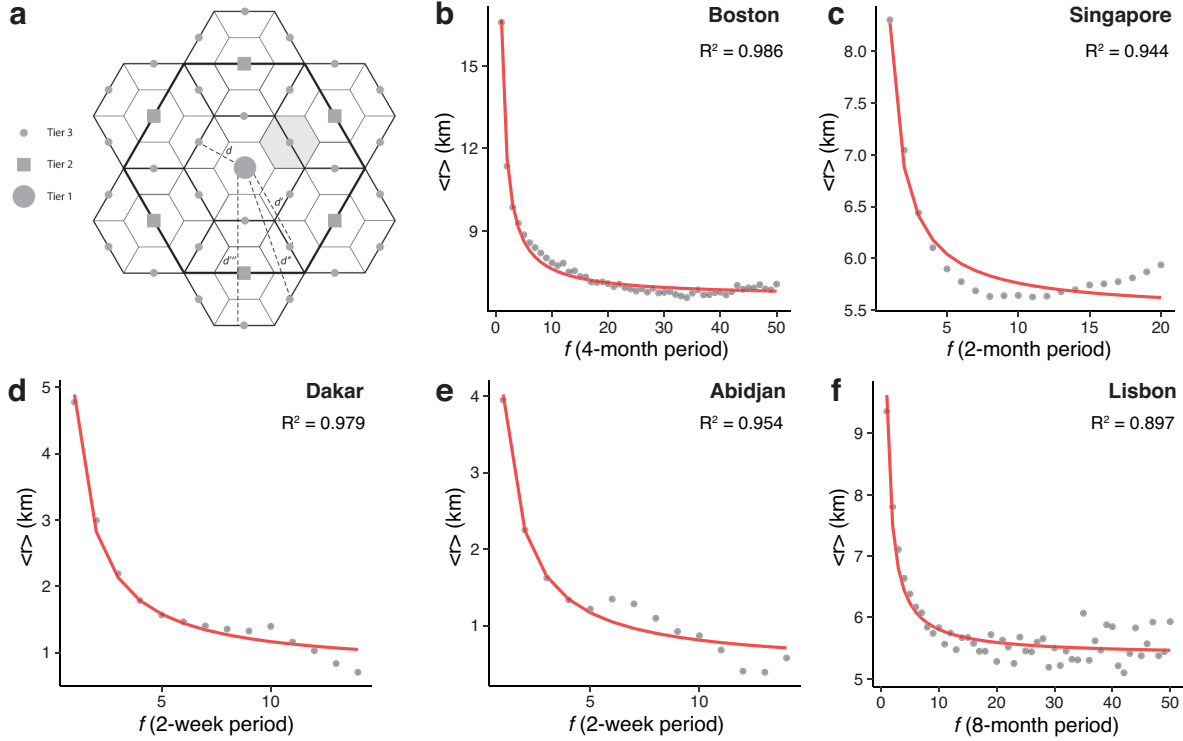
Extended Data Fig. 6 | Universality of the scaling relation $\rho \propto (rf)^{-2}$ across Singapore. The panels depict the data for individual locations (500 m \times 500 m grid cells), ranked according to the total number of visitors from neighbouring cells. Shown are locations of rank 1-30 (from top left to bottom right). The geographic coordinates of each location (latitude and longitude of the centre point of the grid cell) are indicated. The straight lines denote inverse square of rf (slope = -2), consistent with our theoretical argument.



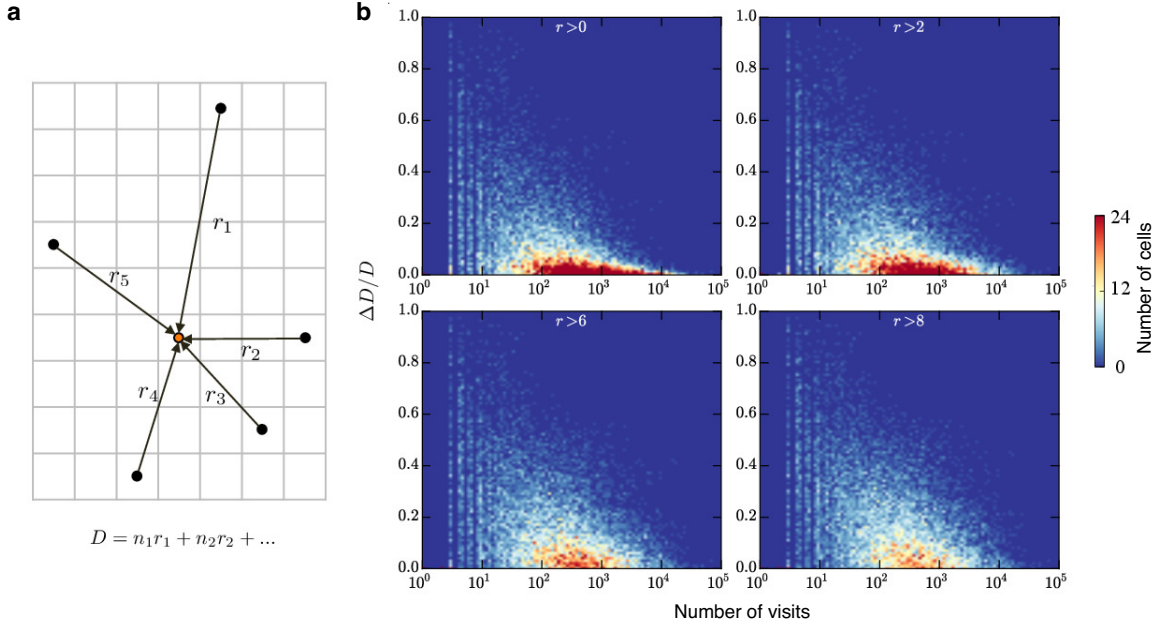
Extended Data Fig. 7 | Simulation results of the EPR model. **a, b,** Generated number of visits (**a**) and attractiveness values μ_i (**b**). **c, d,** The EPR model generates the rf -scaling of the population flows with a scaling exponent that is in remarkable agreement with the data. The generated attractiveness values μ_i are rather homogeneous and uniform across space, which is in contrast to the empirical data. Model parameters are taken from Song et al.³² (Methods).



Extended Data Fig. 8 | Estimation of the magnitude of flows from population density ρ_{pop} . The schematics shows a zoom-in on the immediate vicinity of a destination location j (small values of r), where it is reasonable to assume that $\rho_{\text{pop}}(j) \approx \text{const}$. Hence, the local population density imposes an upper bound on the influx, $\int \rho_j \, df \leq \rho_{\text{pop}}(j)$. A simple boundary condition of the continuous model then dictates that the minimum visiting frequency of all individuals living directly on the boundary (each being assigned to a point at $r = r_j$) assumes the minimum frequency with which the individuals living inside the attracting location return home, $f_{\min} \approx f_{\text{home}}$. The minimum distance r_{\min} for locations from which individuals visit with minimum frequency $f_{\min} < f_{\text{home}}$ increases with decreasing value of f_{\min} .



Extended Data Fig. 9 | Central place theory (CPT) and radius of attraction. **a**, Schematics of CPT, showing the spatial arrangement of three tiers of centres (see Supplementary Information for details). This hierarchical arrangement of central places results in the most efficient transport network. **b, c, d, e, f**, Average travel distance per visit $\langle r \rangle_f$ to perform activities with fixed visiting frequency f across all locations in the studied regions. We find a clear inverse relation, $\langle r \rangle_f \propto 1/f$. The quantity $\langle r \rangle_f$ can be interpreted as the *characteristic distance* associated with the level of specialisation of the functions provided by the locations.



Extended Data Fig. 10 | Fermat-Torricelli-Weber (FTW) efficiency of collective human movements.

a, The schematic figure shows how the FTW efficiency is computed (see Supplementary Information). The effective distance travelled by the visitors of a specific location (cell) can be minimised by moving it on the grid. The efficiency is $\Delta\mathcal{D}/\mathcal{D}$, which is the ratio between the reduction of the effective travel distance of all visitors when moving the cell from its actual location to the optimum FTW point ($\Delta\mathcal{D}$) and the actual effective travel distance of all visitors to that cell (\mathcal{D}). **b**, Density plots representing the number of cells with a given number of visits and FTW efficiency for the Greater Boston Area (for the month of August 2009). The FTW efficiency is computed for each cell based on visits made by visitors who live at distances larger than r_c . For $r_c = 0$ (top left) the density of locations is particularly high where the FTW efficiency is very high. As the number of visits is increased, the distribution becomes narrower and the FTW efficiency increases. This pattern is generally also valid for larger values of r_c but becomes weaker.